Mon. Not. R. Astron. Soc. **379,** 159–168 (2007) doi:10.1111/j.1365-2966.2007.11920.x

NGC 2236: a moderately metal-poor open cluster of Hyades-like age located beyond the Perseus spiral arm

Juan J. Clariá,[1⋆] Andrés E. Piatti,[2⋆] María Celeste Parisi[1⋆] and Andrea V. Ahumada[1⋆]
[1]*Observatorio Astronómico, Universidad Nacional de Córdoba, Laprida 854, 5000 Córdoba, Argentina*
[2]*Instituto de Astronomía y Física del Espacio, CC 67, Suc. 28, Ciudad de Buenos Aires, Argentina*

Accepted 2007 April 25. Received 2007 April 23; in original form 2007 February 27

ABSTRACT

New CCD photometry in the Washington system C and T_1 passbands down to $T_1 \sim 18.5$ mag in the field of the northern open cluster NGC 2236 is presented. T_1 magnitudes and $C - T_1$ colours for a total of 1162 stars within an area of 13.6×13.6 arcmin^2 were measured. These CCD data were supplemented with photoelectric CMT_1T_2 photometry of 13 red giant candidates. The comparison of the cluster (T_1, $C - T_1$) colour–magnitude diagram with theoretical isochrones computed for the Washington system yields $E(C - T_1) = 1.10 \pm 0.10$ and $T_1 - M_{T_1} = 13.45 \pm 0.25$ for $\log t = 8.80$ ($t = 600^{+100}_{-40}$ Myr) and $Z = 0.008$. The derived $E(C - T_1)$ value implies $E(B - V) = 0.55 \pm 0.05$. NGC 2236 is then located at 2.5 ± 0.5 kpc from the Sun beyond the Perseus spiral arm and at ∼10.8 kpc from the Galactic centre. A cluster angular diameter of 9.4 arcmin, equivalent to 6.8 pc, was estimated from star counts both within and outside the cluster field. We also derived from the stellar density profile a cluster core radius of $r_c = 1.7$ arcmin (1.2 pc) and an annular corona of $\Delta r_c = 1.8 r_c$ (2.2 pc). Five independent Washington abundance indices yield a mean cluster metallicity of [Fe/H] $= -0.3 \pm 0.2$, which is not only in reasonably good agreement with the one obtained from the isochrone fit, but also compatible with the existence of a radial abundance gradient in the Galactic disc. We examined the properties of a sample of 20 known open clusters aligned along the line-of-sight to NGC 2236. Berkeley 27 appears as the farthest and oldest cluster of the studied sample.

Key words: techniques: photometric – open clusters and associations: general – open clusters and associations: individual: NGC 2236.

1 INTRODUCTION

Open clusters have a wide range of distances, ages and metallicities. This is why these objects have long been used to probe the formation, structure, dynamics and chemical evolution of the Galactic disc (see e.g. Friel 1995). In particular, open clusters projected towards the Galactic anticentre direction are especially important to study the present and past abundance gradients in the Galactic disc (see e.g. Hou, Chang & Chen 2002, and references therein), while their distribution provides important information about their origin and about the star formation history in the outer Galactic disc (Friel 1995).

The present work is part of a current project of photometric observation in the Washington system of some unstudied or poorly studied open clusters, located in different regions of the Milky Way. We have already reported results based on Washington system CCD photometric observations on the relatively young open clusters NGC 2194 and 2324 (Piatti, Clariá & Ahumada 2003a, 2004b), on the intermediate-age clusters NGC 2627 and Tombaugh 1 (Piatti, Clariá & Ahumada 2003b, 2004c) and on the old metal-poor anticentre cluster Trumpler 5 (Piatti, Clariá & Ahumada 2004a). The present paper is devoted to NGC 2236 (OCL 501, C0627+068), also designated Cr 94 (Collinder 1931). This is an open cluster projected close to the Galactic anticentre direction. We chose to use the Washington system because of its combination of broad-bands, of its high metallicity sensitivity provided by the C filter and of its wide colour baseline between C and T_1 filters. Geisler, Clariá & Minniti (1991, hereafter GCM) and Geisler & Sarajedini (1999) clearly pointed out the advantages offered by this system to derive accurate abundances in yellow and red cluster giants. In particular, high-quality Washington system photoelectric photometry of red giants in several open clusters has recently been used to determine their metal content (see e.g. Clariá et al. 2005; Parisi et al. 2005).

NGC 2236 is located ∼25° from the Galactic anticentre direction in a rich star field in Monoceros at equatorial coordinates

⋆E-mail: claria@mail.oac.uncor.edu (JJC); andres@iafe.uba.ar (AEP); celeste@mail.oac.uncor.edu (MCP); andrea@mail.oac.uncor.edu (AVA)

$\alpha_{2000} = 6^h29^m40^s$, $\delta_{2000} = +6^\circ49\farcm8$ and Galactic coordinates $l = 204\fdg37$, $b = -1\fdg69$. This is a detached, moderately rich of intermediate brightness open cluster of Trumpler class II2m (Archinal & Hynes 2003). Old distance determinations range from 1.6 to 8.3 kpc (Alter, Ruprecht & Vanisek 1970). More recent evidence, however, places this cluster between 2.8 and 3.7 kpc from the Sun. The first study of NGC 2236 was performed by Rahim (1970), who obtained photographic photometry of 280 stars using the *RGU* system and concluded that this group of stars is a cluster with a diameter of about 9 arcmin located at $d = 3430$ pc from the Sun. He also derived $E(G-R) = 0.51$ and $E(G-U) = 0.36$. According to Hawarden (1975), NGC 2236 is at least 400 Myr old. On the basis of *UBV* photographic photometry of 1500 stars brighter than $V = 16.5$, Barkhatova, Orekhova & Shashkina (1988) derived $E(B-V) = 0.46$, $d = 2.8$ kpc and estimated the cluster age to be ∼400 Myr. However, based on photographic and photoelectric photometry of only 39 stars in the cluster field, Babu (1991) derived $d = 3.72$ kpc and estimated a much younger age of 76 Myr. He also reported variable extinction across the cluster field with $E(B-V)$ ranging between 0.68 and 0.84 mag. Phelps, Janes & Montgomety (1994, hereafter PJM) defined the morphological age index δV as the magnitude difference between the main-sequence turn-off and the clump in the (V, $V-I$) colour–magnitude diagram (CMD), deriving $\delta V = 0.4$ for NGC 2236 from their unpublished photometric data. This value implies an age of about 890 Myr (Janes & Phelps 1994), which reveals that the cluster is older than the Hyades. Janes & Phelps (1994) also derived $E(B-V) = 0.37$ and $d = 3.32$ kpc. Adopting $\delta V = 0.4$ and a solar metal content, Salaris, Weiss & Percival (2004) derived an age of 0.86 Gyr from their equation (1). More recently, Loktin, Gerasimenko & Malisheva (2001) determined the following parameters: $E(B-V) = 0.48$, $d = 2930$ pc and $t = 345$ Myr.

NGC 2236 has a comparatively small angular diameter of about 8 arcmin (Lyngå 1987), quite appropriate for CCD camera analysis. Although this cluster was included by PJM in their extensive CCD photometric survey of potentially old open clusters, the photometric data have not yet been published. NGC 2236 is also particularly interesting for the number of red giant candidates it contains as well as for the possibilities these stars provide in terms of cluster metal content derivation. The above-mentioned works prove that there is no agreement on the parameters for NGC 2236, as it has been derived in various studies. Note that the reddening $E(B-V)$ values range from 0.37 (PJM) to 0.84 (Babu 1991), while the ages vary from 76 Myr (Babu 1991) to 890 Myr (Janes & Phelps 1994). We believe that, in view of these remarkable differences, a redetermination of such parameters is worth making on the basis of more reliable data.

In the present study, we report the results obtained from CCD photometry in the C and T_1 passbands of the Washington system up to $T_1 \sim 18.5$ mag in the field of NGC 2236. These data are used to make a new and independent determination of reddening, distance, age and metallicity. In Section 2, we present the observational material and the data reduction, while in Section 3 we examine the photometric errors and describe the main features of the observed CMD. In Section 4, we determine the cluster centre and stellar density radial profile. In Section 5, we determine the cluster fundamental parameters through the fitting of theoretical isochrones computed for the Washington system and apply an independent method to estimate the cluster metallicity. In Section 6, we compare NGC 2236 with those open clusters with known basic parameters projected in nearly the same direction. Section 7 contains a summary of our main conclusions.

2 THE OBSERVATIONAL MATERIAL

2.1 CCD CT_1 photometric data

We obtained CCD images of the cluster field with the Washington C and Kron–Cousins R_{KC} filters and the 0.9-m telescope at Cerro Tololo Inter-American Observatory (CTIO, Chile) during the night of 2004 December 19–20. The recommended prescriptions we used for the C and R_{KC} filters are the ones proposed by Geisler (1996). As Geisler stated, the R_{KC} filter has significant advantages over the standard Washington T_1 filter. From here onwards, we will use indistinctly the words R_{KC} or T_1. The telescope – equipped with the 2048 × 2048 pixel Tektronix 2K No. 3 CCD, with a pixel size of 24 μm – yielded a scale on the chip of 0.4 arcsec pixel^{-1} (focal ratio f/13.5) and a visual field of 13.6 × 13.6 arcmin^2. We controlled the CCD through the CTIO ARCON 3.3 data acquisition system in the standard quad amplifier mode, operating at a mean measured gain (four chips) of 2.00 ± 0.04 e$^-$ ADU^{-1}, with a mean readout noise of 3.60 ± 0.15 e$^-$. Under photometric sky conditions (the typical seeing was 1.1 arcsec), we obtained one 100-s and one 150-s exposures for the C band, and two 10-s exposures for the R_{KC} band. At the beginning of the observing night, we obtained a series of 10 bias and five dome and sky flat-field exposures per filter to calibrate the CCD instrumental signature. In order to standardize our photometry, we carried out observations of standard stars of the Selected Areas PG0231+051, 98 and 101 of Landolt (1992), which cover a wide colour range. In particular, stars in the selected area PG0231+051 were observed at low and high air masses in order to properly adjust the extinction coefficients. At the end of the night, we had collected 34 different measures of magnitude per filter for the selected standard star sample.

We reduced the C, R_{KC} images at the Instituto de Astronomía y Física del Espacio (Argentina) with IRAF[1] using the QUADPROC package. The procedure included the bias subtraction of all the images and the flat-fielding of both standard and program field images; weighted combined signal-calibrator frames were employed. The resulting processed images turned out to be satisfactorily flat. We then derived the instrumental magnitudes for the standard stars from aperture photometry using DAOPHOT/IRAF routines (Stetson, Davis & Crabtree 1990). We obtained the following transformation equations between instrumental and standard magnitudes through least-squares fits:

$$c = (3.727 \pm 0.023) + T_1 + C - T_1 + (0.271 \pm 0.010) \times X_C - (0.080 \pm 0.009) \times (C - T_1), \quad (1)$$

$$r = (3.272 \pm 0.008) + T_1 + (0.089 \pm 0.004) \times X_{T_1} - (0.028 \pm 0.003) \times (C - T_1), \quad (2)$$

where X represents the effective air mass, and capital and lowercase letters stand for standard and instrumental magnitudes, respectively. The coefficients were derived through the IRAF routine FITPARAM, resulting in rms errors of 0.022 for c and 0.009 for r.

The instrumental magnitudes for stars in the NGC 2236 field were obtained from point-spread function (PSF) fits using stand-alone versions of the DAOPHOT[2] and ALLSTAR[2] programs, which provided us with x and y coordinates and instrumental c and r magnitudes for

[1] IRAF is distributed by the National Optical Astronomy Observatories, which is operated by the Association of Universities for Research in Astronomy, Inc., under contract with the National Science Foundation.
[2] Program kindly provided by P.B. Stetson.

all stars identified in each field. The PSFs were generated from two samples of 35–40 and ∼100 stars interactively selected. For each frame, a quadratically varying PSF was derived by fitting the stars in the larger sample, once the neighbours were eliminated by using a preliminary PSF. The PSF was obtained from the smaller star sample, which contained the brightest, least-contaminated stars. We then used ALLSTAR program to apply the resulting PSF to the identified stellar objects and to create a subtracted image, which was used to find and measure magnitudes of additional fainter stars. The PSF magnitudes were determined using the aperture magnitudes yielded by PHOT as zero-points. This procedure was repeated three times for each frame. Next, we computed aperture corrections from the comparison of PSF and aperture magnitudes using the subtracted neighbour PSF star sample. The resulting aperture corrections were −0.01 and 0.00 mag for c and r images, respectively.

Next, we separately combined all the measures for the shorter and longer c, r exposure pairs using the stand-alone DAOMATCH[2] and DAOMASTER[2] programs. We thus obtained two tables which list the running number of stars, the x and y coordinates, the c and r magnitudes, and the respective observational errors for each measured star. Note that stars with only c or r magnitudes were excluded from the tables. The standard magnitudes and colours for all the measured stars were computed through equations (1) and (2). Once we obtained the standard magnitudes and colours, we finally built a master table containing the average of T_1 and $C - T_1$, their errors $\sigma(T_1)$ and $\sigma(C - T_1)$, and the number of observations for each star, respectively. Whenever there was only one measure of T_1 and $C - T_1$, we adopted the corresponding observational error. Table 1 provides the magnitudes and colours for a total of 1162 stars measured in the field of NGC 2236. Only a fragment of this table is presented here as a guidance, regarding its form and content. The complete table, however, is available on the online version of the journal on *Synergy* (see Supplementary Material section). Numbers in the Rahim's (1970) numbering system are given in parenthesis in the first column of Table 1 only for those stars which were observed photoelectrically in the Washington system (see Section 2). Fig. 1 shows a schematic finding chart of the stars observed in the field of NGC 2236. The sizes of the plotting symbols are proportional to the T_1 brightness of the stars. The positions of 12 out of the 13 red giant candidates that we observed photoelectrically in the Washington system using Rahim's (1970) numbering system are identified in the figure. Star 158 falls outside the CCD field of view.

Table 1. CCD CT_1 data of stars in the field of NGC 2236. The full table is available in the online version of the article on *Synergy*.

Star	x (pixel)	y (pixel)	T_1 (mag)	$\sigma(T_1)$ (mag)	$C - T_1$ (mag)	$\sigma(C - T_1)$ (mag)	n
194	667.442	460.639	13.935	0.001	3.021	0.023	2
195	1577.740	465.036	15.992	0.005	1.934	0.001	2
196	155.951	467.211	16.300	0.038	1.004	0.020	2
...	...	...	...	...	...	...	...
...	...	...	...	...	...	...	...

Note. (x, y) coordinates correspond to the reference system of Fig. 1. Magnitude and colour errors are the standard deviations of the mean, or the observed photometric errors for stars with only one measurement. Only for those stars photoelectrically observed, numbers in the Rahim's (1970) numbering system are given in parentheses in the first column.

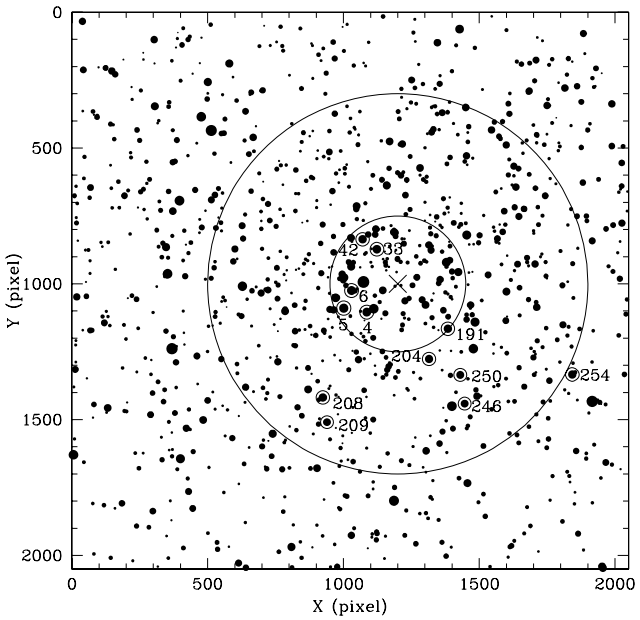

Figure 1. Schematic finding chart of the stars observed in the field of NGC 2236. North is up and east is to the left. The sizes of the plotting symbols are proportional to the T_1 brightness of the stars. Two concentric circles 250 and 700 pixel wide around the cluster centre (*cross*) are shown. 12 of the 13 red giant candidates observed photoelectrically are identified using star numbers from Rahim (1970). Star 158 falls outside the CCD field of view.

2.2 CMT_1T_2 photoelectric data

13 stars brighter than $T_1 = 13.8$ and redder than $C - T_1 = 2.30$ in the cluster field were selected as red giant candidates of NGC 2236. All 13 stars were observed with the C, M, T_1 and T_2 filters of the Washington system (Canterna 1976). The CMT_1T_2 measurements were performed with the CTIO 1.0-m telescope in 1993 January, using a single-channel pulse-counting photometer and a dry-ice cooled Hamamatsu R943-02 GaAs photomultiplier. Only one photoelectric measurement was made for each star. Mean extinction coefficients for CTIO were used, and between 13 and 18 standard stars from the lists of Canterna (1976) and Canterna & Harris (1979) were employed to transform the photoelectric observations into the standard Washington system. A few stars with several precise measurements carried out by Clariá & Lapasset (1985) in the open cluster NGC 5822 were also used as Washington standard stars. The colour transformation slopes show good agreement with those found by Canterna (1976) for CTIO, the resulting mean internal errors of a single observation being 0.009, 0.008, 0.007 for the $C - M$, $M - T_1$ and $T_1 - T_2$ colours, respectively. Table 2 displays the new CMT_1T_2 data for the stars observed. A comparison between the CCD and photoelectric (pe) data obtained for these stars shows excellent agreement, the mean differences being: $\Delta(C-T_1)_{\rm CCD-pe} = -0.002 \pm 0.081$ and $\Delta(T_1)_{\rm CCD-pe} = 0.002 \pm 0.027$.

3 DATA OVERVIEW

In Table 1, we find that 76 per cent of the total number of measured stars have two measures of their $C - T_1$ colours and T_1 magnitudes and range from the brightest magnitude reached – which occurs at $T_1 \approx 12$ mag (confirmed as unsaturated) – down to $T_1 \sim 18$ mag. The remaining measured stars, i.e. 24 per cent of the whole sample,

Table 2. Washington photoelectric photometry of red giant candidates in the field of NGC 2236. Star numbers are from Rahim (1970).

Star	$C-M$	$M-T_1$	T_1-T_2	T_1
4	1.668	1.181	0.849	12.831
5	1.330	1.040	0.742	12.626
6	1.344	1.102	0.783	12.706
33	1.548	1.113	0.796	12.993
42	1.278	1.021	0.748	13.168
158	1.534	1.069	0.800	13.683
191	1.491	1.119	0.779	13.236
204	1.445	1.116	0.794	13.399
208	1.574	1.222	0.855	13.203
209	1.599	1.244	0.874	13.747
246	1.446	1.141	0.825	13.718
250	1.458	1.103	0.807	13.619
254	1.499	1.148	0.810	13.216

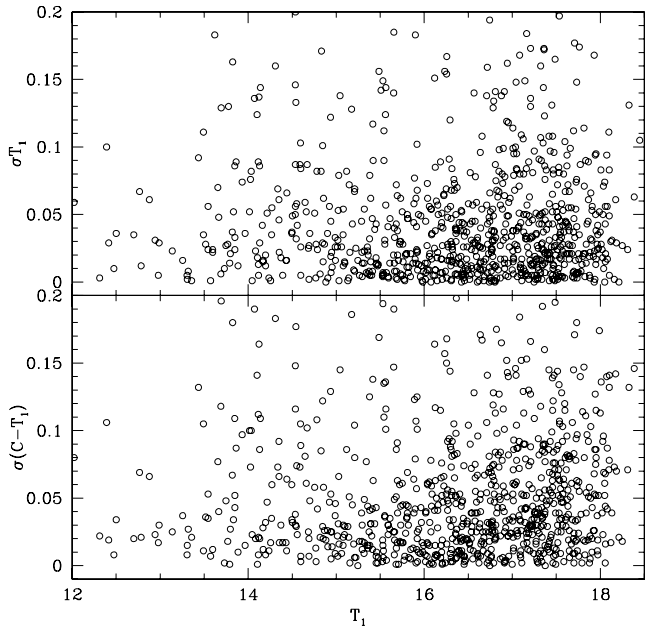

Figure 2. Magnitude and colour photometric errors as a function of T_1.

have only been measured once and most of them have T_1 magnitudes between ∼18.0 and 18.5. Clearly, the ∼6 mag along which our photometry extends in T_1 is mostly covered by stars measured twice. This means that the additional 50 s in the long *c* exposure did not allow us to detect fainter stars. As the long *c* exposure is 50 per cent longer than the short *c* one, we realize that we took good advantage of the whole reachable dynamical magnitude range produced by the combination of the telescope aperture and CCD gain.

In Fig. 2, we plotted the photometric errors provided by the standard deviation of the mean for the T_1 magnitude and $C-T_1$ colours against their corresponding T_1 magnitudes. We used all the stars with two measures taken, since those observed only once have practically no statistical weight. As can be seen, it would seem that a generic dispersion prevails over the expected tendency of increasing the errors as the magnitude grows. However, we can conclude from Fig. 2 that the photometric errors of a randomly selected star are probably smaller than 0.1 mag or, what is more, even smaller than 0.05 mag. Bearing in mind the behaviour of the photometric errors with the magnitude for the observed stars in Fig. 2, we rely on the accuracy

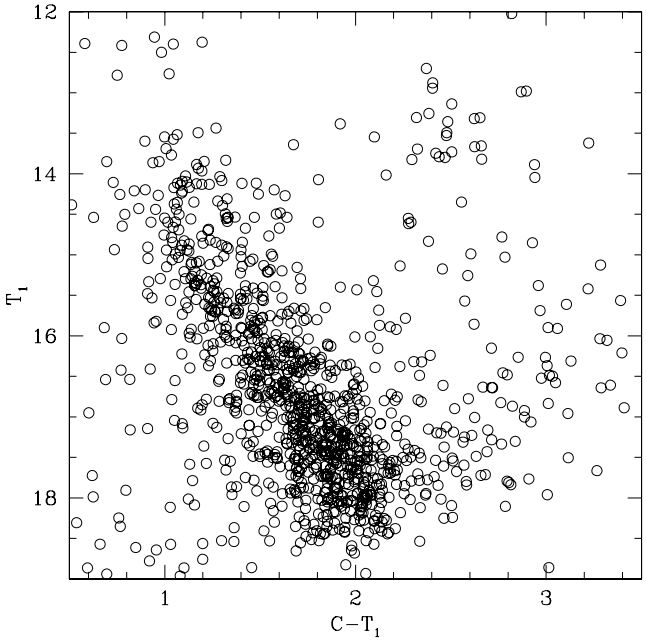

Figure 3. (T_1,$C-T_1$) CMD for stars observed in the field of NGC 2236.

of the morphology and position of the main cluster features in the CMD.

The (T_1, $C-T_1$) CMD obtained using all the measured stars is depicted in Fig. 3. By inspecting this figure, the main cluster features can be identified. What first calls our attention is the cluster main sequence (MS), which looks well populated, has clear signs of evolution and develops along ∼4.5 mag. It is relatively broad, especially in its lower envelope, partly due to field star contamination. The evident hook at the MS turn-off suggests a cluster age of several hundred million years old. On the other hand, a group of stars seems to form the cluster red giant clump (RGC) centred at $T_1 \sim 13.5$ and $C-T_1 \sim 2.5$ mag. This feature increases our suspicion that we are dealing with an intermediate-age open cluster. The width of the cluster's MS does not appear to be the result of photometric errors, since these ones hardly reach a tenth of magnitude at any T_1 level (see above). Therefore, such width could be caused by intrinsic effects (evolution, binarity, etc.) by differential reddening and/or by field star contamination. It must be remembered that field stars also have magnitudes and colours different from those of the cluster's MS.

4 STRUCTURAL CLUSTER FEATURES

The cluster centre can be estimated by examining Fig. 1 with an accuracy varying between 100 and 200 pixels. However, in order to determine such a centre on a more objective and precise basis, we applied a statistical method consisting in tracing the stellar density profiles projected on to the directions of the *x*- and *y*-axes. By fitting those profiles, we obtained the coordinates associated to the geometrical centre. We counted the number of stars distributed along a fixed width band oriented in the direction of the *y*-axis in order to build the *x* projected density profile. Then, we used another band placed along the *x*-axis to construct the *y* projected density profile. The widths of the bands for both directions were chosen to avoid star counts which might include a large number of field stars. For the spatial intervals along the axes, we experimented with bins of 50, 100, 120 and 150 pixel wide. Thus, we could check if there were any

spurious effects caused by the presence of localized groups, rows or columns of stars, and we could select the bin which most appropriately fitted the intrinsic spatial resolution of the observed cluster field. Taking into account the mean-free path between two stars, we looked for neither noisy nor smooth stellar density profiles. Finally, we adopted a bin size of 100 pixel in the subsequent analysis.

The NGAUSSFIT routine of the STSDAS IRAF package was used to fit the projected stellar density profiles, adopting a single Gaussian as the fitting option. We decided to fix the constant and the linear terms to the corresponding background level and to zero, respectively. We used the centre of the Gaussian, its amplitude and its full-width at half-maximum (FWHM) as variables. After eliminating a couple of scattered points, the fitting procedure converged after one iteration on average. The resulting coordinates for the cluster centre turned out to be $(x_c, y_c) = (1200 \pm 50, 1000 \pm 100)$ pixel, which were adopted for the following analysis. The cluster centre is marked by a cross in Fig. 1.

The above-mentioned cluster centre was used as an entry, and then we built the cluster stellar density radial profile by counting the stars located in boxes of 100 pixel a side. By following this method, the number of stars per unit area at a given radius r can be directly calculated through the expression:

$$(n_{r+50} - n_{r-50})/[(m_{r+50} - m_{r-50}) \times 100^2],$$

where n_j and m_j, respectively, represent the number of counted stars and centres of boxes of 100 pixels a side included in a circle of radius j. Thus, we profited from the whole area of the observed field and moved further away from the cluster centre instead of building the radial profile by counting stars within as many complete circles as could be drawn in the observed field. In fact, Fig. 4 shows that the resulting stellar density radial profile reaches up to 1400 pixels away from its centre, whereas the radius of the largest complete circle that can be traced in the observed field is of ∼800 pixel (see Fig. 1). The error bars in the figure represent the estimated uncertainties at various distances from the centre. Each error bar was fixed by comparing two additional radial profiles – constructed following the steps described above but with boxes of 50 and 150 pixel a side, respectively – to the radial profile shown in Fig. 4. It can be seen that the more inwards a radius is, the longer the error bars are due to the non-uniform distribution of cluster stars.

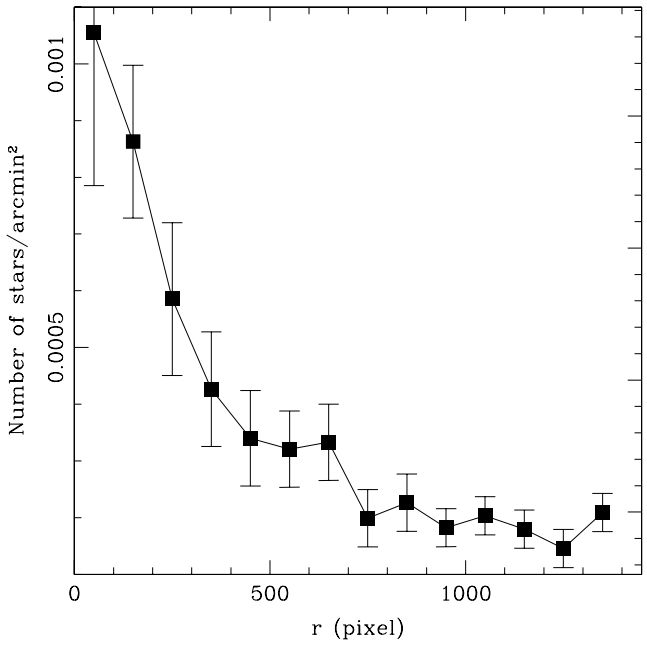

Figure 4. Stellar density radial profile centred at $(x_c, y_c) = (1200, 1000)$ pixel for stars observed in the field of NGC 2236. The horizontal line represents the background level measured for $r > 700$ pixel.

Fig. 4 becomes a valuable tool to estimate the cluster radius, generally used as an indicator of the cluster size, to examine the extension of the cluster core and corona and to establish the area out of which field stars prevail. On using the error bars as a secondary reference, we drew a horizontal line at 0.00021 pixel^{-1}, which resulted from assuming a uniform field star density and from averaging the seven measured outermost points in the figure. From Fig. 4, we also estimated a cluster radius of 700 ± 50 pixel, equivalent to 4.7 ± 0.3 arcmin, and adopted the region for $r > 700$ pixel as the 'star field area'. The derived background level proves to be almost four times lower than the central cluster density. This means that the field star contamination is on average 20 per cent at the cluster centre and grows up to 60 per cent towards the cluster's boundaries. We finally derived a radius of $r_c = 250$ pixel (1.7 arcmin) at half the maximum of the cluster density profile. Therefore, the cluster corona results in an annulus of $\Delta r = 1.8 r_c$. This value does not compare well with the average ratio between the annular width of the corona and the core radius (= 4.3 ± 1.9) found by Nilakshi et al. (2002) for 38 open clusters. However, a larger sample of star clusters is required to understand the cause of this disagreement.

We compared the stellar density radial profile of NGC 2236 with those of other open clusters we observed using both the same CCD and telescope: NGC 2194 (Piatti et al. 2003a); Tr 5 (Piatti et al. 2004a); NGC 2324 (Piatti et al. 2004b); Tombaugh 1 (Piatti et al. 2004c); NGC 6318 (Piatti, Clariá & Ahumada 2005); Lyngå 11 (Piatti, Clariá & Ahumada 2006a); NGC 5288 (Piatti, Clariá & Ahumada 2006b) and NGC 2489 (Piatti et al. 2007). We previously normalized these cluster profiles to the distance and field star density of NGC 2236, and expressed the stellar densities in units of number of stars per square parsec. When the central cluster densities were compared, we found that NGC 2236 does have the highest stellar density, which is 1.8 times larger than those of NGC 6318 (age = 160 Myr) and Trumpler 5 (age = 5 Gyr), and three times larger than those of the remaining clusters. The cluster core radius corresponding to half the maximum of the stellar density radial profile is 1.2 pc, well in the range of the other cluster core radii (1–2 pc), except for NGC 5288 and 2194, whose half maximum density radii are 0.5 and 2.5 pc, respectively. NGC 2236 is as extended as NGC 2194 and 6318 ($r \sim 3.5$ pc). Only NGC 2324 and Trumpler 5 are more extended clusters ($r \sim 5.5$–6.0 pc) than NGC 2236, while the remaining ones are clearly smaller. Regarding its shape, extension and stellar population, we can therefore conclude from the above results that NGC 2236 is a relatively crowded and compact open cluster.

5 CLUSTER FUNDAMENTAL PARAMETER ESTIMATES

Although we cannot identify with absolute certainty which of the photoelectrically observed late-type stars are indeed cluster members, we applied the iterative method described by GCM to determine the cluster metal content.

Our first step was to assume that all the red giant candidates are cluster members and we adopted for these stars a wide range of $E(B - V)$ colour excesses from 0.30 to 0.60, varying every $E(B - V)$ 0.05 mag. $E(B - V)$ colour excesses larger than 0.60 mag lead to unreddened $(T_1 - T_2)$ and $(M - T_2)$ indices for all the red giant candidates outside the range of GCM's calibrations. On the other hand, $E(B - V)$ values smaller than 0.30 mag imply [Fe/H] values

Table 3. Cluster metallicity as a function of reddening. [Fe/H] values in parentheses have been extrapolated.

$E(B-V)$	[Fe/H]
0.30	−1.40
0.35	−1.19
0.40	−0.97
0.45	−0.74
0.50	−0.52
0.55	−0.30
0.60	−0.08
0.65	(0.14)
0.70	(0.36)

which are unacceptably low for an open cluster. Stars 5 and 42 have been omitted in the analysis for $E(B-V) = 0.60$, because in this case both stars fall outside the range of the calibrations given by GCM.

The second step taken to derive metallicity from the Washington colours was to correct the observed Washington indices for reddening, using the reddening ratios given by GCM. According to GCM, the abundance-sensitive index Δ is the difference between the observed colour and the solar abundance colour at the observed $(T_1 - T_2)$ (or $M - T_2$), where all colours refer to unreddened values. GCM described a procedure to correct the decrease in abundance sensitivity as temperature decreases. They also established empirical calibrations of the abundance indices $\Delta'_1 - \Delta'_5$ with [Fe/H], where $\Delta'_1 - \Delta'_5$ refer, respectively, to $\Delta'(C-M)_{T_1-T_2}$, $\Delta'(M-T_1)_{T_1-T_2}$, $\Delta'(C-T_1)_{T_1-T_2}$, $\Delta'(C-M)_{M-T_2}$ and $\Delta'(C-T_1)_{M-T_2}$. These Δ'_i indices can be calculated from the Δ_i indices using GCM's equation (2). Note, however, that $\Delta'_i = \Delta_i$ for all the stars of NGC 2236, provided that the $E(B-V)$ colour excess is larger than 0.40 mag.

Once an $E(B-V)$ value was established, the third step taken consisted in obtaining five different values of the iron-to-hydrogen ratio from the expression:

$$[\mathrm{Fe/H}] = \left[-b_i + \left(b_i^2 - 4a_i\left(c_i - \Delta'_i\right)\right)^{1/2}\right]/2a_i, \qquad (3)$$

where the constants a_i, b_i and c_i are given in GCM's table 10. The five metallicity estimates resulting from each adopted reddening were directly averaged to obtain the cluster metal content. This procedure was repeated for different reddening values in order to examine how the metallicity varies as a function of $E(B-V)$. The results are shown in Table 3, wherein the [Fe/H] values for $E(B-V) \geqslant 0.60$ have been extrapolated. Note in Table 3 that the cluster metallicity strongly depends on the adopted $E(B-V)$ value. In fact, a variation of 0.05 mag in $E(B-V)$ implies a variation of $\sim$0.2 dex in [Fe/H].

Fig. 5 displays the $(C-M)_0$ versus $(T_1-T_2)_0$, $(M-T_1)_0$ versus $(T_1-T_2)_0$, $(C-T_1)_0$ versus $(T_1-T_2)_0$, $(C-M)_0$ versus $(M-T_2)_0$ and $(C-T_1)_0$ versus $(M-T_2)_0$ colour–colour diagrams for the assumed NGC 2236 cluster giants. These were built using the reddening finally adopted for the cluster, i.e. $E(B-V) = 0.55 \pm 0.05$ (see below). The isoabundance relations in Fig. 5 range from [Fe/H] = +0.5 (bottom) to −3.0 (top), in steps of 0.5 dex, except

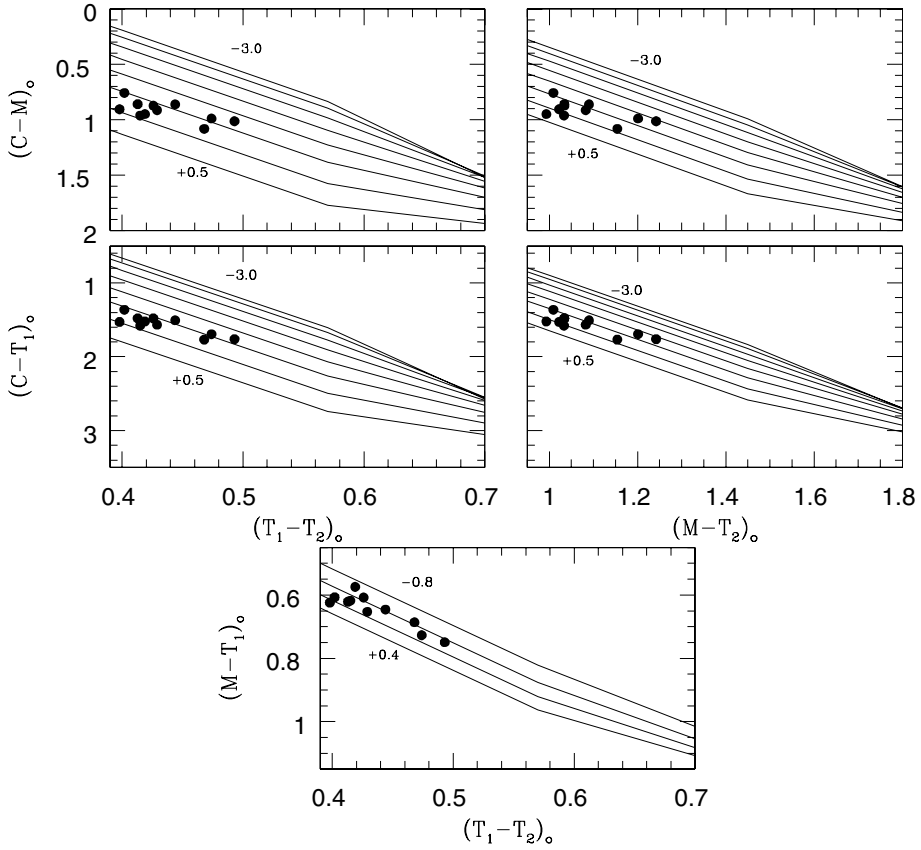

Figure 5. Colour–colour diagrams for the red giant candidates of NGC 2236 corrected by $E(B-V) = 0.55$. Isoabundance relations from GCM for 0.5 dex intervals from [Fe/H] = −3.0 to +0.5 are shown, except for the $(M-T_1)_0/(T_1-T_2)_0$ diagram wherein isoabundance relations for 0.4 dex intervals from [Fe/H] = −0.8 to +0.4 are given. Stars assumed to be red cluster giants are represented with filled circles.

Table 4. Washington abundance-sensitive indices.

Star	Δ'_1	Δ'_2	Δ'_3	Δ'_4	Δ'_5
4	−0.11	−0.05	−0.16	−0.03	−0.05
5	−0.04	0.00	−0.07	−0.01	−0.05
6	−0.18	−0.01	−0.20	−0.15	−0.15
33	−0.03	−0.03	−0.05	+0.02	+0.01
42	−0.12	−0.03	−0.19	−0.05	−0.06
158	−0.06	−0.08	−0.13	+0.07	+0.04
191	−0.02	+0.01	−0.01	−0.02	−0.01
204	−0.12	−0.02	−0.14	−0.08	−0.09
208	−0.22	−0.02	−0.27	−0.19	−0.22
209	−0.27	−0.03	−0.30	−0.23	−0.24
246	−0.24	−0.05	−0.29	−0.16	−0.18
250	−0.16	−0.06	−0.21	−0.07	−0.09
254	−0.13	−0.02	−0.15	−0.10	−0.10

for the $(M - T_1)_0$ versus $(T_1 - T_2)_0$ diagram in which they range from +0.4 to −0.8 in steps of 0.4 dex. The Washington abundance indices Δ'_i computed using $E(B - V) = 0.55$ for the assumed giants are given in Table 4. The resulting mean values and corresponding standard deviations of the mean from 13 assumed giant members are: $\langle\Delta'_1\rangle = -0.13 \pm 0.02$, $\langle\Delta'_2\rangle = -0.03 \pm 0.01$, $\langle\Delta'_3\rangle = -0.17 \pm 0.02$, $\langle\Delta'_4\rangle = -0.08 \pm 0.02$ and $\langle\Delta'_5\rangle = -0.09 \pm 0.02$. These values lead to the following [Fe/H] values and corresponding standard deviations of the mean: $[\mathrm{Fe/H}]_1 = -0.33 \pm 0.06$, $[\mathrm{Fe/H}]_2 = -0.24 \pm 0.05$, $[\mathrm{Fe/H}]_3 = -0.34 \pm 0.06$, $[\mathrm{Fe/H}]_4 = -0.28 \pm 0.09$ and $[\mathrm{Fe/H}]_5 = -0.29 \pm 0.08$. The difference between the abundances derived from the iron lines and those obtained from the blue spectral features contaminated by CN and CH is not overly significant, if we consider the photometric and calibration errors. This fact allows us to conclude that the cluster giants are not enriched by elements of the CNO group. The unweighted average of the five Washington abundance estimates turned out to be $\langle[\mathrm{Fe/H}]\rangle = -0.30 \pm 0.04$. However, since an error of 0.05 mag in $E(B - V)$ translates into an error of ∼0.2 dex in [Fe/H] (see Table 3), we finally adopted $[\mathrm{Fe/H}] = -0.3 \pm 0.2$ for NGC 2236.

Fig. 6 shows the cluster T_1 versus $(C - T_1)$ CMD built using all the measured stars distributed within 700 pixel away from the cluster centre. Although the lower MS is somewhat broad, the relatively long MS, the well-defined MS turn-off and the position of the populous RGC helped us to fit theoretical isochrones in order to derive the $E(C - T_1)$ colour excess, the $T_1 - M_{T_1}$ apparent distance modulus, and the age and metallicity of NGC 2236. We used the theoretical isochrones computed by Girardi et al. (2002) for the Washington system, which include overshooting effect. We would like to remark that convective overshooting considerably changes the cluster ages estimated from isochrone fits. According to Maeder & Meynet (1991) and Bertelli et al. (1994), ages inferred from isochrones without overshooting could be underestimated by 30 per cent for clusters younger than 1–2 Gyr.

We selected here three different subsets of isochrones – log t between 8.0 and 9.2 – with $Z = 0.008$, 0.020 and 0.040, respectively, which cover the metallicity range of most of the Galactic open clusters studied in detail (Chen, Hou & Wang 2003). We independently fitted each isochrone and obtained the corresponding $E(C - T_1)$ colour excesses and $T_1 - M_{T_1}$ apparent distance moduli. Next, we filled in a grid with four columns containing the assumed Z value (= 0.008, 0.020 and 0.040), the log t of the respective selected isochrone, and the $E(C - T_1)$ and the $T_1 - M_{T_1}$ values obtained for each (Z, log t) pair. Then, we obtained the $E(B - V)$ values corresponding to $Z = 0.008$, 0.020 and 0.040 ([Fe/H] = −0.40, 0.0 and 0.30) by interpolation among values in Table 3. After this, we entered with these $E(B - V)$ values in the grid to derive log t and $T_1 - M_{T_1}$ for each of the three Z values. The expression $E(C - T_1) = 1.97\ E(B - V)$ (Geisler 1996) was used to relate both colour excesses.

Finally, we superimposed the three selected isochrones (one for each Z value), and adopted one of them in turn – the one which best reproduced the cluster MS features and RGC locus – as representative of the cluster age and metal content. Note that isochrones of various metallicities did not yield negligible differences in the CMD adjustments. The isochrone of $\log t = 8.80$ ($t = 600$ Myr) and $Z = 0.008$ turned out to be the one which most accurately reproduces the cluster features in the $(T_1, C - T_1)$ CMD. To match this isochrone, we used a $E(C - T_1)$ colour excess and a $T_1 - M_{T_1}$ apparent distance modulus of 1.10 and 13.45, respectively. The uncertainties of these parameters were estimated from the cluster features dispersion. We thus estimated $\sigma(E(C - T_1)) = 0.10$ mag, $\sigma(T_1 - M_{T_1}) = 0.25$ mag and $\sigma(t) = {}^{+100}_{-40}$ Myr. In Fig. 6, we overlapped the zero-age main sequence (ZAMS) and the isochrone of $\log t = 8.80$ (solid lines) for $Z = 0.008$ on the cluster CMD. The dashed lines in the figure correspond to the isochrones of $\log t = 8.70$ and 8.90, which were included for comparison purposes. Filled circles in Fig. 6 represent the red giant candidates photoelectrically observed in the Washington system.

Note that the loop in the isochrone corresponding to the bluest stage during the He-burning core phase is shifted redwards by about $\Delta(C - T_1) \approx 0.2$ mag, equivalent to $\Delta(B - V) \approx 0.10$ mag, in relation to the observed position of the cluster RGC. Theoretical RGCs have also frequently proved to be redder than the observed ones in previous studies of star clusters whose ages span from 0.3 to 2.3 Gyr (Geisler et al. 2003; Piatti et al. 2003a). Nevertheless, some

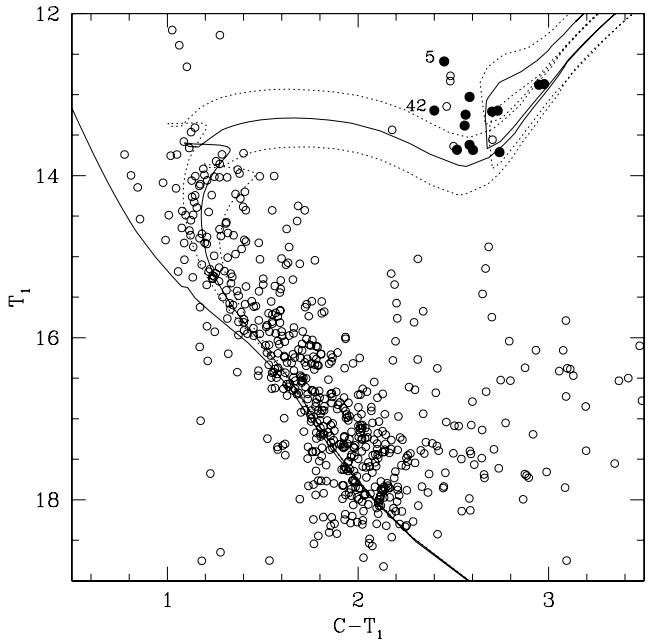

Figure 6. $r < 700$ pixel $(T_1, C - T_1)$ CMD for stars in NGC 2236. The ZAMS and the isochrone of $\log t = 8.80$ from Girardi et al. (2002), computed taking into account overshooting and $Z = 0.008$, are overplotted. We included in dashed lines the isochrones for $\log t = 8.70$ and 8.90, for comparison purposes. The filled circles represent the cluster giant candidates observed with CMT_1T_2 photoelectric photometry. Stars 5 and 42 fall slightly outside the range of the GCM's calibrations.

other studies found good agreement between theory and observations regarding the positions of RGCs in intermediate-age clusters (Clariá, Mermilliod & Piatti 1999; Mermilliod et al. 2001). Based on the comparison of empirical and Padova isochrones, Piatti, Clariá & Bica (1998) confirmed the existence of a shift between the positions of the observed loops and the theoretically predicted ones for clusters older than 200 Myr.

From the expressions $E(C - T_1) = 1.97\ E(B - V)$ and $M_{T_1} = T_1 + 0.58E(B-V) - (V - M_V)$ given by Geisler (1996), we obtained $E(B - V) = 0.55 \pm 0.05$ and $V - M_V = 13.8 \pm 0.3$ mag. Therefore, the cluster metal content derived from the photoelectric CMT_1T_2 data turns out to be [Fe/H] $= -0.3 \pm 0.2$ (see Table 3). We would like to point out that although in this case stars 5 and 42 fall slightly outside the range of the GCM's abundance calibrations, we did include them in the cluster metallicity determination. If the isoabundance lines in Fig. 5 are barely extrapolated, the positions of both stars in the five Washington colour–colour diagrams imply [Fe/H] ≈ -0.3. This fact leads us to believe that both stars are very likely giant cluster members.

Using the most frequently accepted value for the $A_V/E(B - V)$ ratio (Straizys 1992), we obtain a true distance modulus $V_o - M_V = 12.0 \pm 0.4$, which implies a distance from the Sun of 2.5 ± 0.5 kpc and a height out of the Galactic plane of 74 pc. The distance error was computed through the expression: $\sigma(\mathrm{d}) = 0.46 \times [\sigma(V - M_V) + 3.2 \times \sigma(E(B - V))] \times \mathrm{d}$, where $\sigma(V - M_V)$ and $\sigma\ (E(B - V))$ represent the estimated errors in $V - M_V$ and $E(B - V)$, respectively. By using the cluster Galactic coordinates (l, b) and the calculated cluster distance, we derived (10.78, −1.03, −0.07) kpc and ∼10.8 kpc for the cluster (X, Y, Z) coordinates and Galactocentric distance, respectively, assuming the Sun's distance from the centre of the Galaxy to be 8.5 kpc.

6 AN UPDATED PICTURE OF NGC 2236

The position of NGC 2236, its interstellar extinction, its age and its here-derived metallicity do seem to be in very good agreement with the generally accepted picture of the structure and chemical evolution of the Galactic disc. To confirm such assertion, we first searched for clusters located at $(l, b)_{\mathrm{cluster}} = (l, b)_{\mathrm{NGC\,2236}} \pm 5^\circ$ in order to examine the interstellar absorption law along the line-of-sight to NGC 2236. We used the WEBDA Open Cluster Data base (Mermilliod & Paunzen 2003), because its periodical updates make it an excellent tool to analyse cluster samples. WEBDA provided us with 31 identified open clusters in the above-mentioned direction, even when 20 of them have already known distances from the Sun, $E(B - V)$ colour excesses and ages (Table 5). Only three out of those 20 clusters have abundance estimates. The result of the search shows that further work is required to increase the number of detailed studies on Galactic open clusters.

The cluster reddening and its distance from the Sun here derived place NGC 2236 among the relatively most reddened and distant known open clusters projected towards the direction considered, a result which is illustrated in Fig. 7. It is also of great value to learn – whenever possible – how metallicity and age distributions vary for different Galactic longitude intervals. This is due to the fact that usually we trace gradients of determined parameters as a function of Galactocentric distance, which may sometimes hide peculiar behaviours. The upper left hand panel of this figure shows the distribution of the selected clusters (filled circles) and NGC 2236 (filled triangle) in the Galactic (X, Y) plane. Note that the Sun is assumed to be located at $(X, Y) = (8.5, 0)$. We traced with solid lines a Sun-centred circle of radius 2 kpc as well as the Perseus spiral arm (Drimmel & Spergel 2001). Note that the distance between the outermost and the innermost clusters is nearly 4.7 kpc. The upper right hand panel in Fig. 7 shows the relationship between the visual interstellar absorption A_V and the distance d from the Sun. For the sake of comparison, we also included the relationship between A_V and d corresponding to the Baade's Window [$(l,\ b) = (1^\circ,\ -3\overset{\circ}{.}9)$] – not far from the direction considered here – obtained by Ng et al. (1996), which is represented by a solid line. It can be perceived from both panels that the presence of the Perseus spiral arm – schematically drawn in the figure – causes a large dispersion in the interstellar absorption A_V values in the direction considered. In fact, the visual absorption affecting clusters located between 1 and 2 kpc from the Sun is found to range from practically unreddened up to ∼2.3 mag. Moreover, most of the selected clusters belong to the Galactic plane (see bottom left hand panel), while Berkeley 27 – the furthest open cluster in the sample located at 5 kpc from the Sun and at a height of 0.23 kpc out of the Galactic plane (Hasegawa et al. 2004) – is only slightly reddened. According to Hasegawa et al. (2004), Berkeley 27 is 2.0 Gyr old; it is therefore the oldest cluster of the present sample (bottom right hand panel). The Hyades-like age (600 Myr) of NGC 2236, its position in the Galactic disc ($R_{\mathrm{GC}} = 10.8$ kpc) and its metallicity ([Fe/H] $= -0.3$) are consistent with both the existence of a radial abundance gradient ranging from −0.07 to −0.10 dex kpc^{-1} in the Galactic disc and the age–metallicity relation so far delineated by Friel (1995).

Table 5. Fundamental parameters for clusters projected in the direction towards NGC 2236.

Cluster	l (°)	b (°)	$E(B-V)$ (mag)	d (kpc)	Z (kpc)	age (Myr)	R_{GC} (kpc)
NGC 2259	201.76	2.08	0.59	3.30	0.120	316	11.64
Cr 95	201.81	0.03	0.10	0.56	0.000	229	9.02
Tr 5	202.87	1.05	0.58	3.00	0.060	4075	11.32
NGC 2264	202.94	2.20	0.05	0.67	0.030	10	9.12
NGC 2186	203.55	−6.19	0.27	1.45	−0.160	55	9.84
NGC 2251	203.57	0.11	0.19	1.33	0.000	270	9.73
NGC 2202	203.62	−4.90	0.00	0.90	−0.080	550	9.33
Basel 8	203.78	−0.12	0.37	1.33	0.000	126	9.73
Basel 7	203.82	0.53	0.40	1.68	0.020	110	10.06
NGC 2254	204.33	0.05	0.40	2.36	0.000	204	10.70
Platais 6	205.30	−6.19	0.00	0.35	−0.040	62	8.82
Cr 97	205.37	−1.76	0.00	0.63	−0.020	100	9.07
Cr 106	206.03	−0.41	0.23	1.60	−0.010	5	9.96
NGC 2244	206.31	−2.07	0.46	1.45	−0.050	8	9.82
ASSC 26	206.35	3.06	0.13	0.80	0.040	123	9.22
Cr 107	207.15	−0.89	0.54	1.74	−0.030	10	10.08
Berkeley 27	207.78	2.60	0.05	5.04	0.230	1995	13.17
NGC 2269	207.89	0.30	0.40	1.69	0.010	263	10.02
Cr 96	207.96	−3.39	0.51	0.96	−0.060	11	9.36
vdBergh 1	208.56	−1.81	0.71	1.69	−0.050	107	10.01

7 SUMMARY AND CONCLUSIONS

In this study, we present CCD photometry in the Washington system C and T_1 passbands of 1162 stars in the field of the open cluster NGC 2236. We also present here CMT_1T_2 photoelectric photometry of 13 red giant candidates. The analysis of the photometric data leads to the following main conclusions:

(i) The (T_1, $C - T_1$) CMD reveals a somewhat broad and relatively long cluster MS and a populous clump of He-burning red

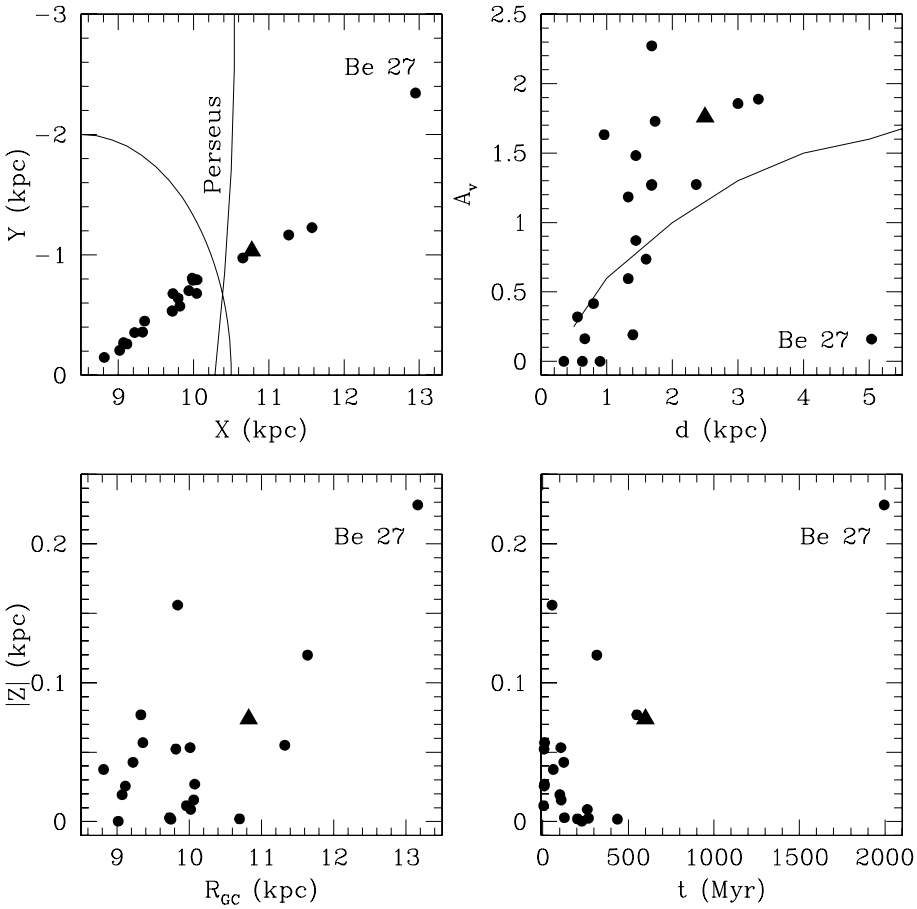

Figure 7. The relationship between the Galactic coordinates X and Y (upper left), between the distance d from the Sun and the visual interstellar absorption A_V (upper right), between the Galactocentric distance R_{GC} and the height $|Z|$ out of the Galactic plane (bottom left), and between $|Z|$ and age (bottom right) for known open clusters projected in the line-of-sight to NGC 2236. Selected clusters and NGC 2236 are represented by filled circles and by a filled triangle, respectively. A Sun-centred circle of radius 2 kpc and the Perseus spiral arm are shown in the upper left hand panel. The relationship between d and A_V for Baade's Window is indicated in the upper right hand panel.

giant stars. Photometric errors do not seem to be responsible for the observed broadness of the cluster MS. The most probable cause of the MS blurring seems to be intrinsic effects (evolution, binarity, etc.), differential reddening and/or star field contamination. We estimate that the field star contamination is, on average, 20 per cent at the cluster centre and increases up to 60 per cent in the cluster boundaries.

(ii) Star counts carried out in 100 pixel a side boxes distributed through the whole observed field allowed us to derive an angular radius of 4.7 arcmin, equivalent to 3.4 pc. From the cluster stellar density radial profile, we also derived a cluster core radius of $r_c = 1.7$ arcmin (1.2 pc) and an annular corona of $\Delta r = 1.8\ r_c$ (2.2 pc).

(iii) Estimates of the cluster fundamental parameters were made from the comparison of the observed (T_1, $C - T_1$) CMD with theoretical isochrones of the Padova group computed for the Washington system. The following values were derived for the reddening, apparent distance modulus, age and metallicity: $E(C - T_1) = 1.10 \pm 0.10$, $T_1 - M_{T_1} = 13.45 \pm 0.25$, $t = 600^{+100}_{-40}$ Myr and $Z = 0.008$. NGC 2236 is then a Hyades-like age cluster located at 2.5 ± 0.5 kpc from the Sun beyond the Perseus spiral arm, at 70 pc out of the Galactic plane and at $\sim$10.8 kpc from the Galactic centre.

(iv) A metal abundance [Fe/H] $= -0.3 \pm 0.2$ relative to the Sun was determined from the Washington system photoelectric photometry of 13 probable red giant members, in good agreement with the value inferred from the best fit of isochrones. This [Fe/H] value places NGC 2236 in the metal-poor side of the metallicity distribution of the Galactic open clusters. Spectroscopic observations of the red cluster giants will be of great importance to confirm the metallicity here derived. Therefore, they are strongly recommended. The cluster Galactocentric position and metallicity appear to be compatible with the existence of a radial abundance in the Galactic disc.

(v) An inspection of the properties of 20 known open clusters aligned along the line-of-sight to NGC 2236 as seen from the Sun reveals that Berkeley 27 is the farthest and oldest cluster of the sample. It can also be seen that the Perseus spiral arm causes a large dispersion in the visual interstellar absorption values, affecting the clusters located between 1 and 2 kpc from the Sun.

ACKNOWLEDGMENTS

We are gratefully indebted to the CTIO staff for their hospitality and support during the observing run. The present work was partially supported by the Argentinian institutions CONICET, Agencia Nacional de Promoción Científica y Tecnológica (ANPCyT) and Agencia Córdoba Ciencia. This work is based on observations made at Cerro Tololo Inter-American Observatory (CTIO), which is

operated by AURA, Inc., under cooperative agreement with the National Science Foundation.

REFERENCES

Alter G., Ruprecht J., Vanisek J., 1970, Catalogue of Star Clusters and Associations. Akademiai Kiado, Budapest

Archinal B. A., Hynes S. J., 2003, Star Clusters. Willman-Bell, Richmod, VA

Babu G. S. D., 1991, JA&A, 12, 187

Barkhatova K. A., Orekhova L. K., Shashkina L. P., 1988, SvA, 32, 18

Bertelli G., Bressan A., Chiosi C., Fagoto F., Nasi E., 1994, A&AS, 106, 275

Canterna R., 1976, AJ, 81, 228

Canterna R., Harris H. C., 1979, in Philip A. G. D., ed., Problems of Calibration and Multicolour Photometric Systems. Dudley Observatory, Schenectady, NY, p. 199

Chen L., Hou J. L., Wang J. J., 2003, AJ, 125, 1397

Clariá J. J., Lapasset E., 1985, MNRAS, 214, 229

Clariá J. J., Mermilliod J.-C., Piatti A. E., 1999, A&AS, 134, 301

Clariá J. J., Piatti A. E., Lapasset E., Parisi M. C., 2005, Baltic Astron., 14, 301

Collinder P., 1931, Medd. Lunds Astron. Obs., 2

Drimmel R., Spergel D. N., 2001, ApJ, 556, 181

Friel E. D., 1995, ARA&A, 33, 81

Geisler D., 1996, AJ, 111, 480

Geisler D., Sarajedini A., 1999, AJ, 117, 308

Geisler D., Clariá J. J., Minniti D., 1991, AJ, 102, 1836 (GCM)

Geisler D., Piatti A. E., Bica E., Clariá J. J., 2003, MNRAS, 341, 771

Girardi L., Bertelli G., Bressan A., Chiosi C., Groenewegen M. A. T., Marigo P., Salasnich B., Weiss A., 2002, A&A, 391, 195

Hasegawa T., Malasan H. L., Kawakita H., Obayashi H., Kurabayashi T., Nakai T., Hyakkai M., Arimoto N., 2004, PASJ, 56, 295

Hawarden T., 1975, MNRAS, 173, 231

Hou J.-L., Chang R.-X, Chen J. J., 2002, Chin. J. Astron. Astrophys., 1, 17

Janes K. A., Phelps R. L., 1994, AJ, 108, 1773

Landolt A., 1992, AJ, 104, 340

Loktin A., Gerasimenko T., Malisheva L., 2001, A&A Trans., 20, 605

Lyngå G., 1987, Catalogue of Open Cluster Data, Centre de Données Stellaires, Strasbourg

Maeder A., Meynet G., 1991, A&AS, 89, 451

Mermilliod J.-C., Clariá J. J., Andersen J., Piatti A. E., Mayor M., 2001, A&A, 375, 30

Mermilliod J.-C., Paunzen E., 2003, WEBDA Open Cluster Database. A&A, 410, 511

Ng Y. K., Bertelli G., Chiosi C., Bressan A., 1996, A&A, 310, 771

Nilakshi S. R., Pandey A. K., Mohan V., 2002, A&A, 383, 153

Parisi M. C., Clariá J. J., Piatti A. E., Geisler D., 2005, MNRAS, 363, 1247

Phelps R. L., Janes K. A., Montgomery K. A., 1994, AJ, 107, 1079 (PJM)

Piatti A. E., Clariá J. J., Ahumada A. V., 2003a, MNRAS, 340, 1249

Piatti A. E., Clariá J. J., Ahumada A. V., 2003b, MNRAS, 346, 390

Piatti A. E., Clariá J. J., Ahumada A. V., 2004a, MNRAS, 418, 979

Piatti A. E., Clariá J. J., Ahumada A. V., 2004b, A&A, 421, 991

Piatti A. E., Clariá J. J., Ahumada A. V., 2004c, MNRAS, 349, 641

Piatti A. E., Clariá J. J., Ahumada A. V., 2005, PASP, 117, 22

Piatti A. E., Clariá J. J., Ahumada A. V., 2006a, New Astron., 11, 262

Piatti A. E., Clariá J. J., Ahumada A. V., 2006b, MNRAS, 367, 599

Piatti A. E., Clariá J. J., Bica E., 1998, ApJS, 116, 263

Piatti A. E., Clariá J. J., Mermilliod J.-C., Parisi M. C., Ahumada A. V., 2007, MNRAS, 377, 1737

Rahim M., 1970, A&A, 9, 221

Salaris M., Weiss A., Percival S. M., 2004, A&A, 414, 163

Stetson P. B., Davis L. E., Crabtree D. R., 1990, in ASP Conf. Ser. Vol. 8, CCDs in Astronomy. Astron. Soc. Pac., San Francisco, p. 289

Straizys V., 1992, Multicolor Stellar Photometry. Pachart Publishing House, Tucson, Arizona

SUPPLEMENTARY MATERIALS

The following supplementary material is available for this article:

Table 1. CCD CT_1 data of stars in the field of NGC 2236.

This material is available as part of the online article from:

http://www.blackwell-synergy.com/doi/abs/10.1111/j.1365-2966.2007.11920.x

(This link will take you to the article abstract.)

Please note: Blackwell Publishing are not responsible for the content or functionality of any supplementary materials supplied by the authors. Any queries (other than missing material) should be directed to the corresponding author for the article.

This paper has been typeset from a TEX/LATEX file prepared by the author.